NASA Technical Paper 2375

January 1985

Transonic Flow Analysis for Rotors

Part 2—Three-Dimensional, Unsteady, Full-Potential Calculation

I-Chung Chang

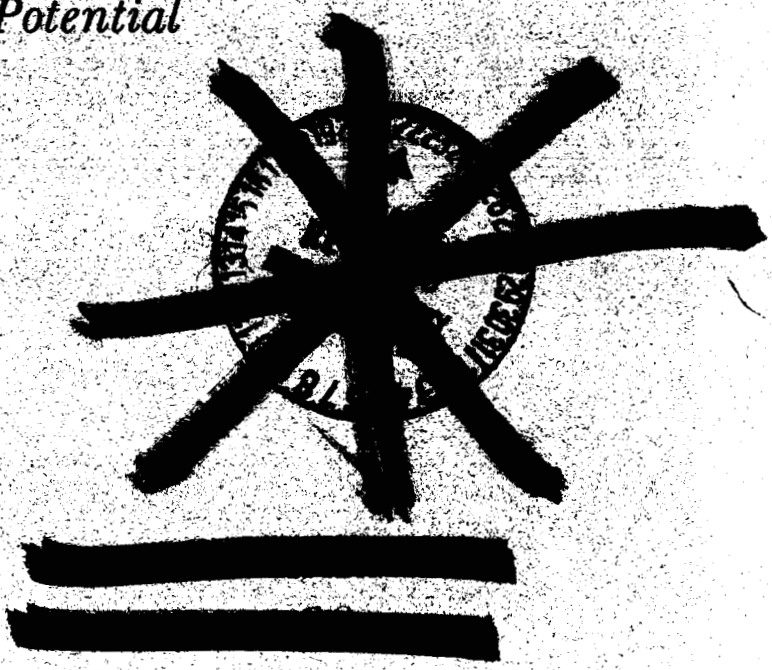

NASA

NASA Technical Paper 2375

1985

Transonic Flow Analysis for Rotors

Part 2—Three-Dimensional, Unsteady, Full-Potential Calculation

I-Chung Chang

Ames Research Center
Moffett Field, California

National Aeronautics and Space Administration

Scientific and Technical Information Branch

SYMBOLS

a	local speed of sound, m/sec
CD	drag coefficient of a profile
CL	lift coefficient of a profile
CM	moment coefficient of a profile (with respect to quarter-chord point)
CP	pressure coefficient
M	local Mach number
P	pressure
R	rotor radius, m
r/R	relative radius of blade station
t	time, sec
U_∞	wind velocity in the wind tunnel, m/sec
x/c	chordwise relative position on a profile
α_o	incidence, deg
γ	ratio of specific heats (1.4 for air)
μ	advance ratio ($U/\Omega R$)
ρ	density
ϕ	velocity-potential in the inertial frame
$[\phi]$	jump in velocity-potential
ψ	blade azimuthal position, deg
Ω	angular velocity of the rotor, rad/sec

SUMMARY

A numerical method is presented for calculating the three-dimensional unsteady, transonic flow past a helicopter rotor blade of arbitrary geometry. The method solves the full-potential equations in a blade-fixed frame of reference by a time-marching implicit scheme. At the far-field, a set of first-order radiation conditions is imposed, thus minimizing the reflection of outgoing wavelets from computational boundaries. Computed results are presented to highlight radial flow effects in three dimensions, to compare surface pressure distributions to quasi-steady predictions, and to predict the flow field on a swept-tip blade. The results agree well with experimental data for both straight- and swept-tip blade geometries.

INTRODUCTION

The exact flow fields around helicopter rotor blades are generally acknowledged to be complex, unsteady, and three-dimensional. Problems arise because of strong flow separation on the retreating blade and because of transonic effects on the advancing blade. The present study is concerned with the advancing blade, the tip of which may enter the transonic flow regime and the aerodynamic coefficients of which may change appreciably as a result of transient shock-wave movements. Accurate predictions of these shock motions are essential preconditions to further improvement of the helicopter rotor blade. The difficulty and expense of obtaining such detailed flow information experimentally are sufficient reasons for developing a computational method for characterizing the flow.

All previous computer codes for handling these flows have involved small disturbance on mean surface approximations (refs. 1-5). The most advanced of these codes is an alternating-direction, implicit solution scheme for the low-frequency, unsteady, transonic small-disturbance equations. In the present study, the flow physics is modeled by the unsteady, transonic full-potential equations; this modeling allows more realistic specification of the blade geometry, and should provide better resolution of the associated flow phenomena. The numerical method for two-dimensional airfoils, developed in reference 6, was extended to calculate three-dimensional, unsteady rotor flows.

This is Part II of a series of planned publications under the same general title "Transonic Flow Analysis for Rotors."

HELICOPTER ROTOR FLOW FIELD

Before discussing the details of the numerical model, it is worthwhile to discuss, in general terms, helicopter rotor flow fields. The helicopter rotor blade generates an extremely complex flow. The combination of forward speed and uniform rotation causes each blade section to encounter a sinusoidally varying free-stream velocity. In addition, to avoid rolling moments, blade incidence is varied nearly sinusoidally throughout each blade revolution. The result is a very complicated

aerodynamic environment. Figure 1, taken from reference 7, was obtained by a calculation based on an acceleration potential method; it shows contours of constant Mach number, constant-sweep angle, and constant incidence over the rotor disk.

GOVERNING EQUATIONS

In order to develop an accurate, efficient, and reliable computer code that can be used for engineering purposes, the flow modeling is based on potential-flow theory. The shock wave is therefore assumed to be weak enough so that the entropy jump across it is negligible. In other words, the flow is assumed to be inviscid and isentropic over the entire flow field. A velocity potential ϕ exists for the flow and is described in a frame of reference that is at rest relative to the undisturbed air. In this inertial frame, the complete equation for the velocity potential is

$$\phi_{tt} + [(\vec{\nabla}\phi)^2]_t + \vec{\nabla}\phi \cdot \vec{\nabla}\left[\frac{1}{2}(\vec{\nabla}\phi)^2\right] = a^2\nabla^2\phi$$

where a is the local speed of sound. Bernoulli's equation, relating a and ϕ, is

$$\phi_t + \frac{1}{2}(\vec{\nabla}\phi)^2 + \frac{a^2}{\gamma - 1} = \frac{a_\infty^2}{\gamma - 1}$$

where a_∞ is the sound speed in the undisturbed air, and γ is the specific heat ratio (1.4 for air).

If the blade geometry and location are described by $S(\vec{r};t) = 0$, where $\vec{r}$ is the position vector in the inertial frame, then the boundary condition at the blade surface is

$$S_t + \vec{\nabla}\phi \cdot \vec{\nabla}S = 0$$

For further analysis it is more convenient to implement this surface boundary condition in a moving frame of reference in which the blade location is fixed. Let primed variables refer to the inertial frame F' and unprimed variables refer to the blade-fixed moving frame F. Suppose that at time t, the two frames are coincident and that F is moving relative to F' with a linear velocity $\vec{U}$ and an angular velocity $\vec{\Omega}$. Then, at that time t, the position vector $\vec{r}$ of a particular fluid particle is the same for both frames. If a point P is rigidly fixed in F', it appears to an observer in F to move with velocity $\vec{V} = -(\vec{U} + \vec{\Omega} \times \vec{r})$. Thus, the velocity of fluid particle at P in F is $\vec{q} = \vec{\nabla}\phi + \vec{V}$. The rate of change of ϕ at P is measured by an observer in F as

$$\phi_{t'} = \phi_t + \vec{V} \cdot \vec{\nabla}\phi$$

The potential equation in the moving frame F is given by

$$\phi_{tt} + 2\vec{V} \cdot \vec{\nabla}\phi_t + (\vec{V} \cdot \vec{\nabla})(\vec{V} \cdot \vec{\nabla}\phi) + \vec{\nabla}\phi \cdot \vec{V}_t + 2\vec{\nabla}\phi \cdot \vec{\nabla}\phi_t + (\vec{V} \cdot \vec{\nabla})[(\vec{\nabla}\phi)^2] + \vec{\nabla}\phi \cdot \vec{\nabla}\left[\frac{1}{2}(\vec{\nabla}\phi)^2\right] = a^2\nabla^2\phi$$

and Bernoulli's equation is

$$\phi_t + \vec{V} \cdot \vec{\nabla}\phi + \frac{1}{2} (\nabla\phi)^2 + \frac{a^2}{\gamma - 1} = \frac{a_\infty^2}{\gamma - 1}$$

Let the moving frame F be described in a Cartesian coordinates system in which x, y, and z represent the chordwise, vertical, and spanwise directions of the blade, respectively, and the origin of which is at the center of rotation. In the inertial frame, let the advance velocity $\vec{U}$ lie in the (x',y') plane and let it make an inclination angle α_o with the negative x'-axis direction, and let the angular velocity $\vec{\Omega}$ be in the positive y'-axis direction. The velocity $\vec{V}$ owing to the motion of the moving frame F has the components

$$V_1 = \Omega z + U \cos \alpha_o \sin \psi$$

$$V_2 = U \sin \alpha_o$$

and

$$V_3 = -\Omega x + U \cos \alpha_o \cos \psi$$

where ψ is the azimuthal angle of the blade ($\psi = 180°$ for forward flight direction in the inertial frame).

The potential equation in Cartesian coordinates is

$$\phi_{tt} + 2q_1\phi_{xt} + 2q_2\phi_{yt} + 2q_3\phi_{zt}$$

$$= (a^2 - q_1^2)\phi_{xx} + (a^2 - q_2^2)\phi_{yy} + (a^2 - q_3^2)\phi_{zz} - 2q_1q_2\phi_{xy} - 2q_1q_3\phi_{xz} - 2q_2q_3\phi_{yz}$$

$$+ (\Omega^2 x - 2\Omega U \cos \alpha_o \cos \psi)\phi_x + (\Omega^2 z + 2\Omega U \cos \alpha_o \sin \psi)\phi_z \qquad (1)$$

where q_1, q_2, and q_3 are the velocity components of local fluid particle in the moving frame and are specified as

$$q_1 = \phi_x + V_1$$

$$q_2 = \phi_y + V_2$$

and

$$q_3 = \phi_z + V_3$$

Bernoulli's equation in Cartesian coordinates is

$$\phi_t + V_1\phi_x + V_2\phi_y + V_3\phi_z + \frac{1}{2} (\phi_x^2 + \phi_y^2 + \phi_z^2) + \frac{a^2}{\gamma - 1} = \frac{a_\infty^2}{\gamma - 1} \qquad (2)$$

Several boundary conditions are necessary to complete the boundary value problem. In the near-field, the flow tangency to the blade is described by the expression

$$\vec{q} \cdot \vec{n} = 0$$

where $\vec{n}$ is the unit vector normal to the blade surface. A simple rectilinear wake model is used here. The wake that is shed from the trailing edge is assumed to be a vortex sheet that is a smooth continuation of the trailing edge. Across this vortex sheet, normal and binormal velocity components and pressure are assumed to be continuous. The jump in potential determined at the trailing edge of each spanwise profile is then assumed to propagate to infinity according to the wake condition

$$[\phi_t] + \vec{q}_m \cdot \vec{\nabla}[\phi] = 0 \tag{3}$$

where $\vec{q}_m$ stands for the mean of upper and lower velocities at each point on the vortex sheet. At the far-field, the boundary condition can be formulated as a Neumann condition so that the time-derivatives of the velocity potential along the characteristics of the flow equation in each spanwise plane vanish. Mathematically, it is subject to the condition

$$\phi_t + \vec{q}_a \cdot \vec{\nabla}\phi = 0 \tag{4}$$

where $\vec{q}_a$ is the outgoing eigen-velocity of the flow equation in each spanwise plane (ref. 6).

MESH SYSTEM

A parabolic sheared mesh system (refs. 8-12) is used in the present analysis. The blade surface is conformal with a coordinate surface of this system. Thus, it is easy to include the blade surface condition in a finite-difference calculation. The mesh system is generated by a series of transformations from the physical space to the computational domain; it is briefly described here in the interest of completeness.

The shearing transformation- The shearing transformation,

$$\bar{x} = x - x_s(z)$$

$$\bar{y} = y - y_s(z)$$

and

$$\bar{z} = z$$

shears out the blade sweep and dihedral. The point $x_s(z)$, $y_s(z)$ is the center of the circle passing through three points near the leading edge of the profile at each spanwise station.

The scaling transformation- The scaling transformation,

$$\tilde{x} = \bar{x}/\mathrm{SCAL}$$

$$\tilde{y} = \bar{y}/\mathrm{SCAL}$$

and

$$\tilde{z} = \bar{z}/\mathrm{SCALZ}$$

accounts for the scaling between the physical space and the computational domain; SCAL and SCALZ are real variables, which accounts for the scaling between the physical space and the computational domain.

The square-root transformation- The square-root transformation,

$$(X_1 + iY_1)^2 = 2(\tilde{x} + i\tilde{y})$$

and

$$Z_1 = \tilde{z}$$

maps the entire blade surface to a shallow bump $Y_1 = S(X_1,Z_1)$ near the plane $Y_1 = 0$.

The second shearing transformation- The second shearing transformation,

$$X = X_1$$

$$Y = Y_1 - S(X_1,Z_1)$$

and

$$Z = Z_1$$

reduces the blade surface to a portion of the plane $Y = 0$.

The stretching transformations- The stretching transformations are introduced to render the computational domain finite. For example,

$$Y = \frac{b\bar{Y}}{(1 - \bar{Y}^2)^a}, \quad 0 < a < 1 \quad \text{and} \quad b > 0$$

is used to map the planes $Y = \pm\infty$ to $Y = \pm 1$. Similar transformations are used outboard of the blade tips in the Z-direction and downstream of the trailing edge in the X-direction.

The flow equation (1) in the computational domain is very complicated and will not be repeated here (the reader is referred to ref. 11 for details). There is a degenerate case. For points on the continuation of the singular line outboard of the blade tips, where the Jacobian vanishes, the potential equation reduces to a simple, two-space-dimensional Laplace equation.

FINITE-DIFFERENCE SCHEME

The time-marching scheme developed in reference 6 for two-space-dimensional problems will be extended to three-space-dimensional problems. The scheme is of three time-levels, with time-levels $n - 1$ and n predicting time level $n + 1$. There is no iteration in any of the time-marching procedures. Basically, the velocity components at each grid point are evaluated by using central differencing at time-level n. The time-derivative term in Bernoulli's equation is evaluated by backward difference.

It is convenient to have the following difference operators: D central difference operator, $\overleftarrow{D}$ upwind difference operator, and $\bar{D}$-type difference operator. To be specific, the definitions of operators acting in the x-direction are given by the following:

1. Central difference operator:

$$D_x\phi_i = (\phi_{i+1} - \phi_{i-1})/(2\Delta x)$$

2. Upwind difference operator (forward or backward):

$$q_1\overleftarrow{D}_x\phi_i = \begin{cases} q_1 \cdot (\phi_i - \phi_{i-1})/(\Delta x) & \text{if} \quad q_1 > 0 \\ q_1 \cdot (\phi_{i+1} - \phi_i)/(\Delta x) & \text{if} \quad q_1 < 0 \end{cases}$$

3. Type-dependent difference operator:

$$\bar{D}_x = \begin{cases} D_x & \text{for subsonic points} \\ \overleftarrow{D}_x & \text{for supersonic points} \end{cases}$$

The second-order difference operators are defined as combinations of the above difference operators; namely, $D_{xy} = D_xD_y$, etc.

Flow Equation

The potential-flow equation in canonical form is

$$\phi_{tt} + 2(\vec{q} \cdot \nabla)\phi_t = (a^2 - q^2)\phi_{ss} + a^2(\nabla^2\phi - \phi_{ss}) + \text{first-order terms} \qquad (5)$$

where s is the local streamwise direction unit vector. Its finite-difference approximation can be described as the following. For the left-hand side of the above equation, upwind differences are used for all spacial derivatives, and central difference is used for all temporal derivatives; namely,

$$\phi_{tt} + 2q_1\phi_{xt} + 2q_2\phi_{yt} + 2q_3\phi_{zt}$$

$$\approx (\phi^{n+1} - 2\phi^n + \phi^{n-1})/(\Delta t)^2 + (q_1\overleftarrow{D}_x + q_2\overleftarrow{D}_y + q_3\overleftarrow{D}_z)(\phi^{n+1} - \phi^{n-1})/(\Delta t)$$

Here, we add some convection viscosity through upwind differences which stabilizes the scheme but introduces some dissipation. The desired ability to capture shocks automatically requires the introduction of viscosity in the differencing of the right-hand side of equation (5). This is done by means of Jameson's rotated difference scheme (refs. 8-11). That is, for contributions to ϕ_{ss}, type-dependent differences are used for all spacial derivatives, and the term ϕ^n is replaced by the arithmetic mean of ϕ^{n+1} and ϕ^{n-1}:

$$\phi_{ss} = \frac{1}{q^2}\left(q_1^2\phi_{xx} + q_2^2\phi_{yy} + q_3^2\phi_{zz} + 2q_1q_2\phi_{xy} + 2q_1q_3\phi_{xz} + 2q_2q_3\phi_{yz}\right)$$

$$\approx \frac{1}{2q^2}\left(q_1^2\bar{D}_{xx} + q_2^2\bar{D}_{yy} + q_3^2\bar{D}_{zz} + 2q_1q_2\bar{D}_{xy} + 2q_1q_3\bar{D}_{xz} + 2q_2q_3\bar{D}_{yz}\right)(\phi^{n+1} + \phi^{n-1})$$

For contributions to $\nabla^2\phi - \phi_{ss}$, central differences are used for all spacial derivatives, and the term ϕ^n is again replaced by the mean of ϕ^{n+1} and ϕ^{n-1}. For the first-order terms in the right-hand side of equation (5), central differences are used for all spacial derivatives. Finally, the finite-difference approximation to the whole flow equation can be written as

$$(\phi^{n+1} - 2\phi^n + \phi^{n-1})/(\Delta t)^2 + (q_1\overleftarrow{D}_x + q_2\overleftarrow{D}_y + q_3\overleftarrow{D}_z)(\phi^{n+1} - \phi^{n-1})/(\Delta t)$$

$$= (a^2 - q^2)/(2q^2)(q_1^2\bar{D}_{xx} + q_2^2\bar{D}_{yy} + q_3^2\bar{D}_{zz} + 2q_1q_2\bar{D}_{xy} + 2q_1q_3\bar{D}_{xz} + 2q_2q_3\bar{D}_{yz})$$

$$\cdot (\phi^{n+1} + \phi^{n-1}) + a^2/(2q^2)[(q_2^2 + q_3^2)D_{xx} + (q_1^2 + q_3^2)D_{yy} + (q_1^2 + q_2^2)D_{zz}$$

$$- 2q_1q_2D_{xy} - 2q_1q_3D_{xz} - 2q_2q_3D_{yz}](\phi^{n+1} + \phi^{n-1})$$

$$+ (\Omega^2 x - 2\Omega U\cos\alpha_o\cos\psi)D_x\phi^n + (\Omega^2 z + 2\Omega U\cos\alpha_o\sin\psi)D_y\phi^n$$

The discretization error associated with the finite-difference approximation is of second order in space for subsonic points and first order in space for supersonic points and second order in time. The system of algebraic equations generated by the finite-difference equation is large. However, this equation can be factored within the same order of accuracy. The following factorization has been tested and found to be stable with time-steps much larger than the time-step allowed by the CFL condition for an explicit scheme.

Let $M = q/a$; then

$$L_x = 1 + \Delta t q_1\overleftarrow{D}_x + \frac{\Delta t^2}{2}q_1^2\bar{D}_{xx} - \frac{\Delta t^2}{2M^2}(q_1^2\bar{D}_{xx} + q_2^2D_{xx} + q_3^2D_{xx})$$

$$L_y = 1 + \Delta t q_2\overleftarrow{D}_y + \frac{\Delta t^2}{2}q_2^2\bar{D}_{yy} - \frac{\Delta t^2}{2M^2}(q_1^2D_{yy} + q_2^2\bar{D}_{yy} + q_3^2D_{yy})$$

and

$$L_z = 1 + \Delta t q_3\overleftarrow{D}_z + \frac{\Delta t^2}{2}q_3^2\bar{D}_{zz} - \frac{\Delta t^2}{2M^2}(q_1^2D_{zz} + q_2^2D_{zz} + q_3^2\bar{D}_{zz})$$

Then the approximate factorization of the finite-difference equation can be written as

$$L_xL_yL_z\phi^{n+1} = \text{RHS}$$

Here RHS consists of the terms involving ϕ^n and ϕ^{n-1} in the above finite-difference equation. This factorization reduces the large complicated matrix inversion problem to three one-dimensional problems. The solution algorithm can be expressed as

$$L_x X = RHS$$

$$L_y Y = X$$

and

$$L_z \phi^{n+1} = Y$$

Each of the above steps required a penta-diagonal matrix solver because second-order upwind difference operators are used in each of the difference operators L.

Radiation Boundary Condition

The artificial radiation boundary condition (eq. (4)) is of the form

$$\phi_t + \bar{u}\phi_x + \bar{v}\phi_y + \bar{w}\phi_z = 0$$

which is approximated by

$$(\phi^{n+1} - \phi^{n-1})/(2\Delta t) + (\bar{u}\overleftarrow{D}_x + \bar{v}\overleftarrow{D}_y + \bar{w}\overleftarrow{D}_z)(\phi^{n+1} + \phi^{n-1})/2 = 0$$

Again, it can be factored as

$$(1 + \Delta t\bar{u}\overleftarrow{D}_x)(1 + \Delta t\bar{v}\overleftarrow{D}_y)(1 + \Delta t\bar{w}\overleftarrow{D}_z)\phi^{n+1} = RHS$$

The algorithm consists of the following three steps:

$$(1 + \Delta t\bar{u}\overleftarrow{D}_x)X = RHS$$

$$(1 + \Delta t\bar{v}\overleftarrow{D}_y)Y = X$$

and

$$(1 + \Delta t\bar{w}\overleftarrow{D}_z)\phi^{n+1} = Y$$

Wake Condition

If the wake of each blade section is assumed to lie on the x-axis, the wake condition is

$$[\phi_t] + \bar{u}_m[\phi_x] = 0$$

where $\bar{u}_m$ is the mean of upper and lower wake velocities. The finite-difference approximation is given by

$$\frac{[\phi_i^n] - [\phi_i^{n-1}]}{\Delta t} + \bar{u}_m \cdot \frac{[\phi_i^n] - [\phi_{i-1}^n]}{\Delta x} = 0$$

Let $b = u_m \Delta t / \Delta x$; then

$$[\phi_i^n] = \frac{[\phi_i^{n+1}] + b[\phi_{i-1}^n]}{1 + b}$$

Hence, once the jump at the trailing edge has been found, the jump in the entire wake can be calculated from the above formula.

RESULTS AND DISCUSSION

A new computer code that contains both quasi-steady and unsteady modes has been developed. The quasi-steady mode is based on the theory reported in reference 11, and the unsteady mode is based on the above theory. Good results can be obtained on mesh containing 128 × 24 × 32 grid points in the chordwise, vertical, and spanwise directions, respectively. On the Ames' Cray 1-S computer, it takes about 40 sec of CPU time for the quasi-steady mode to calculate each azimuthal position and about 30 min CPU time for the unsteady mode to calculate a half rotor revolution, from 0° to 180° (with 0.25° per time-step). Further improvement in computing speed can be realized through a more complete vectorization of the code. The capability of the computer code is demonstrated through the following studies.

Radial Flow Effect

First the quasi-steady mode was used to obtain radial flow effect. Two quasi-steady calculations were performed on the same ONERA, nonlifting, straight-tip rotor blade (ref. 12) at azimuthal angles of 60° and 120°, respectively. At these azimuthal positions, the chordwise flow components are equal, but the radial flow components point outward and inward, respectively. The advance ratio was 0.55 (U_∞ = 110 m/sec and ΩR = 200 m/sec) for both calculations. Figure 2 compares the calculated pressure distributions at span stations r/R = 0.85, 0.9, and 0.95. The radial flow effect is more prominent near the blade tip, which further confirms that three-dimensional modeling must be used to calculate rotor-flow phenomena. It is also worth noting that for a blade section at the outboard portion of the blade, the negative sweep (ψ = 120°) tends to attenuate the expansion at the leading edge and, hence, to reduce the supersonic zone and the intensity of the recompression shock.

Unsteady Effect

For the same straight-tip rotor blade, figure 3 compares unsteady, quasi-steady, and ONERA-measured surface-pressure distributions at the three different span stations (r/R = 0.85, 0.9, and 0.95) for azimuthal angles from 30° to 180° at 30° increments. The advance ratio was 0.55 (U_∞ = 110 m/sec and ΩR = 200 m/sec). The agreement between unsteady calculations and test data is generally very good. A time retardation of the shocks owing to unsteadiness is indicated in the following comparison: (1) the shock at 120° azimuth is stronger than that at 90° azimuth in both the unsteady calculation and the ONERA measurement; (2) the quasi-steady calculation predicts no shock at 150° azimuth, whereas the unsteady calculation catches the shock measured in the experiment; and (3) the quasi-steady calculations predict stronger shock waves in the first quadrant and weaker shockwaves in the second quadrant. This comparison shows that the quasi-steady theory does not adequately predict the strong

shock waves that persist over a range of azimuthal angles at extremely high advance ratios. Further comparison was made at a lower advance ratio (0.4) for the same rotor blade. Figure 4 shows the comparison among unsteady, quasi-steady, and test surface pressure distributions. Agreement is quite good for this case in which the flows are either subsonic or subcritical with very weak shock waves. It is also noted that the quasi-steady theory gives very good pressure predictions for a rotor blade near 90° azimuth for flow with moderate shocks and is useful for design work.

Planform Geometry

To illustrate the capability of predicting the flow on realistic rotor blades, an unsteady calculation was performed for a nonlifting ONERA swept-tip blade (ref. 12) at an advance ratio of 0.5 (U_∞ = 105 m/sec, ΩR = 210 m/sec). This swept-tip blade geometry has a kink at $r/R = 0.85$, with a 30° sweep angle. Figure 5 shows the comparison between unsteady results and ONERA test data. Again, the correlation is quite good. The code accounts for the non-straight leading edge and its effect on the pressure distributions. Figure 6 shows the evolution with azimuth angle of the pressure coefficients at some chordwise points in the same span section. The comparison of full-potential computed results (at $x/c = 0.3$ and $r/R = 0.915$) and ONERA test data ($x/c = 0.293$ and $r/R = 0.911$) reveals that full-potential theory, even with equations in nonconservative form, is able to predict the transient shock position and hence the shock moving speed. However, the shock strength is slightly overpredicted, a common result for an inviscid, full-potential calculation.

CONCLUSIONS

A finite-difference method for predicting the three-dimensional, unsteady transonic flow over a nonlifting helicopter rotor blade in forward flight was presented. The method solves the unsteady, transonic, full-potential equations in nonconservative form in a blade-fixed mesh system in which the blade surface is conformal with a coordinate surface; the system is particularly suitable for modeling the geometry effect of the blade. The code based on this method is shown to be a useful tool for analyzing unsteady aerodynamics of helicopter rotors. Like its quasi-steady companions (ref. 11), the unsteady code has several desirable features; for example,

1. The capability of treating blades of nearly arbitrary geometry

2. The capability of predicting flow over a blade at any azimuthal angle

3. The option to restrict calculations to the flow over the outboard portion of the blade for computational efficiency

Computed results obtained from this new code were compared with ONERA data for both straight- and swept-tip blades. Good comparison between experimental and theoretical pressure distributions of blades could be obtained in transonic flows. It is concluded that

1. The transonic phenomena taking place on the tip of a rotor blade in nonlifting regime are basically three-dimensional and unsteady

2. The quasi-steady theory predicts good unsteady pressure distributions for a rotor blade in flow which is either entirely subsonic or subcritical with very weak shocks

3. The quasi-steady theory gives good pressure distributions for a rotor blade near 90° azimuth for flow with moderate shock waves; thus, it is useful for design work

4. The unsteady theory is necessary to predict unsteady transonic load for a rotor blade in flow that is either supercritical or transonic with moderate shock waves

5. The full-potential equations do not necessarily have to be cast in conservation form to catch the transient shock wave movements

The extension of the method to the lifting rotor blade depends on a good wake modeling. For a prescribed wake, the simple model used in reference 13 should be a good candidate. For a free wake, a suitable model for transonic potential flow equations appears to be a very difficult problem.

Ames Research Center
National Aeronautics and Space Administration
Moffett Field, California 94035, June 13, 1984

REFERENCES

1. Caradonna, F. X.; and Isom, M. P.: Subsonic and Transonic Potential Flow over Helicopter Rotor Blades. AIAA J., vol. 10, Dec. 1972, pp. 1606-1612.

2. Caradonna, F. X.; and Isom, M. P.: Numerical Calculations of Unsteady Transonic Potential Flow over Helicopter Rotor Blades. AIAA J., vol. 14, Apr. 1976, pp. 428-488.

3. Caradonna, F. X.; and Phillipe, J. J.: The Flow over a Helicopter Blade Tip in the Transonic Regime. Vertica, vol. 2, 1978, pp. 43-60.

4. Grant, J.: The Prediction of Supercritical Pressure Distributions on Blade Tips of Arbitrary Shape over a Range of Advancing Blade Azimuth Angles. Proceedings of the 4th European Rotorcraft and Powered Lift Aircraft Forum, Vol. I, Construzioni Aeronautiche Agusta S.p.A., 1978, pp. 2-0 to 2-10.

5. Chattot, J. J.: Calculation of Three-Dimensional Unsteady Transonic Flows past Helicopter Blades. NASA TP-1721, 1980.

6. Chang, I. C.: Unsteady Transonic Flow past Airfoils in Rigid Body Motion. Ph.D. Dissertation, Courant Institute of Mathematical Sciences, New York U., 1980 (also published as a Courant Report DOE/ER/03077-170, Mar. 1981).

7. Philippe, J. J.; and Chattot, J. J.: Experimental and Theoretical Studies on Helicopter Blade Tips at ONERA. ONERA TP No. 1980-96, 6th European Rotorcraft and Powered Lift Aircraft Forum, U. of Bristol, Bristol, England, Sept. 1980.

8. Jameson, A.; and Caughey, D.: Numerical Calculation of the Transonic Flow past a Swept Wing. Courant Institute of Mathematical Sciences, New York U., C003077-140, 1977 (also NASA CR-153297, 1977).

9. Arielli, R.; and Tauber, M.: Computation of Subsonic and Transonic Flow about Lifting Rotor Blades. AIAA Paper 79-1667, Aug. 1979.

10. Chang, I. C.; and Tauber, M.: Numerical Calculation of the Transonic Potential Flow past a Cranked Wing. NASA TM-84391, 1983.

11. Chang, I. C.: Transonic Flow Analysis for Rotors. Part 1: Three-Dimensional Quasi-Steady Full-Potential Calculation. NASA TP-2375, 1984.

12. Tauber, M. E.; Chang, I. C.; Caughey, D. A.; and Philippe, J. J.: Comparison of Calculated and Measured Pressures on Straight- and Swept-Tip Model Rotor Blades. NASA TM-85872, 1983.

13. Caradonna, F. X.; Desopper, A.; and Tung, C.: Finite-Difference Modeling of Rotor Flows Including Wake Effects. Eighth Congress Europeen sur les Helicopteres, Aix-en-Provence, France, 1982.

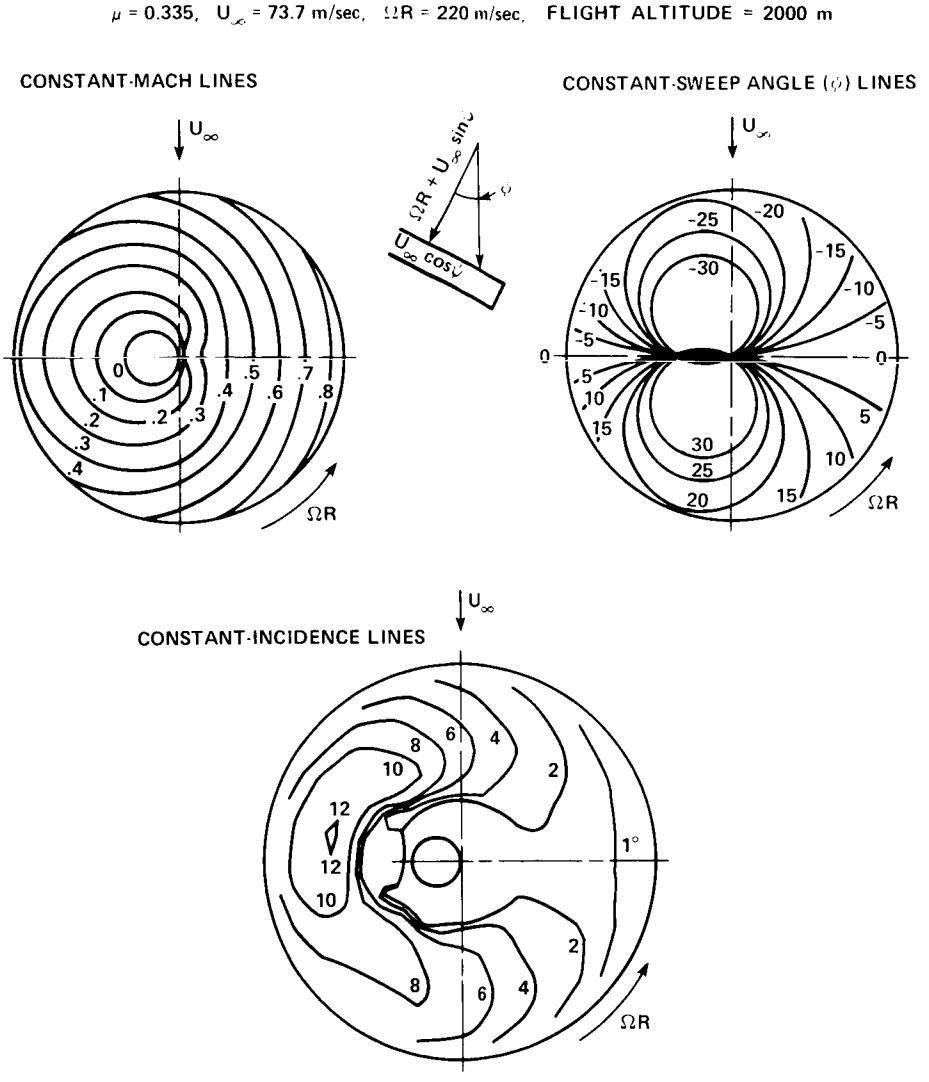

Figure 1.- Constant-Mach number, constant-sweep angle, and constant incidence contours on a rotor disk.

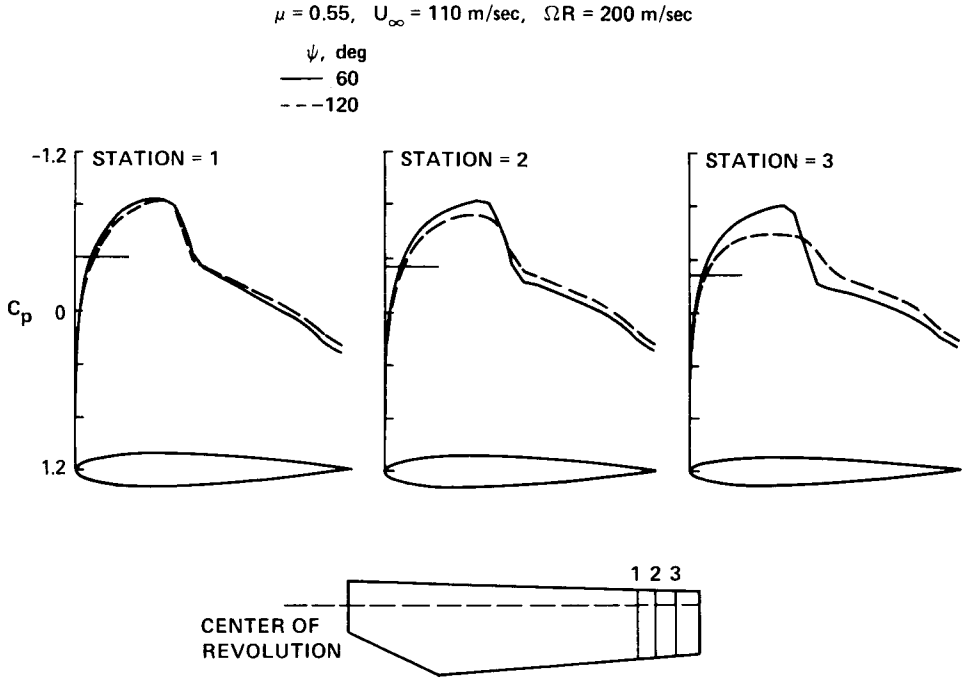

(a) Comparison of surface-pressure distributions at three span stations near the tip of a model rotor blade at azimuthal positions, 60° and 120°.

Figure 2.- Radial flow effect.

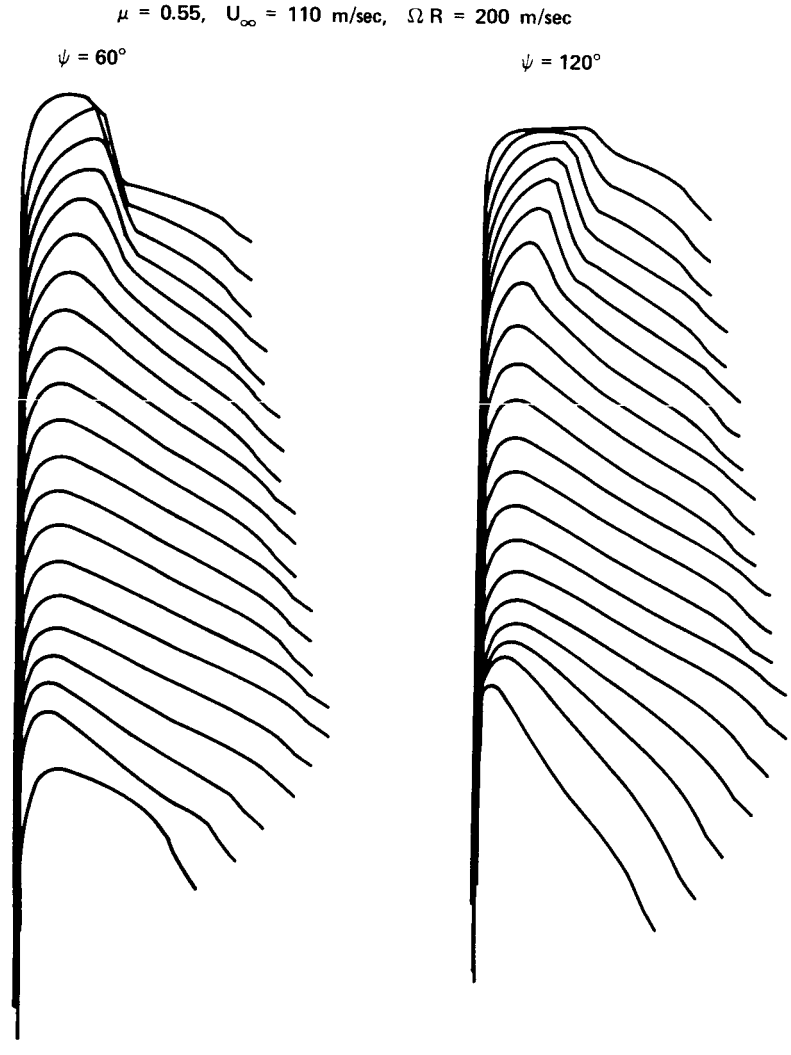

(b) Three-dimensional surface-pressure distributions of a model rotor blade at azimuthal positions, 60° and 120°.

Figure 2.- Concluded.

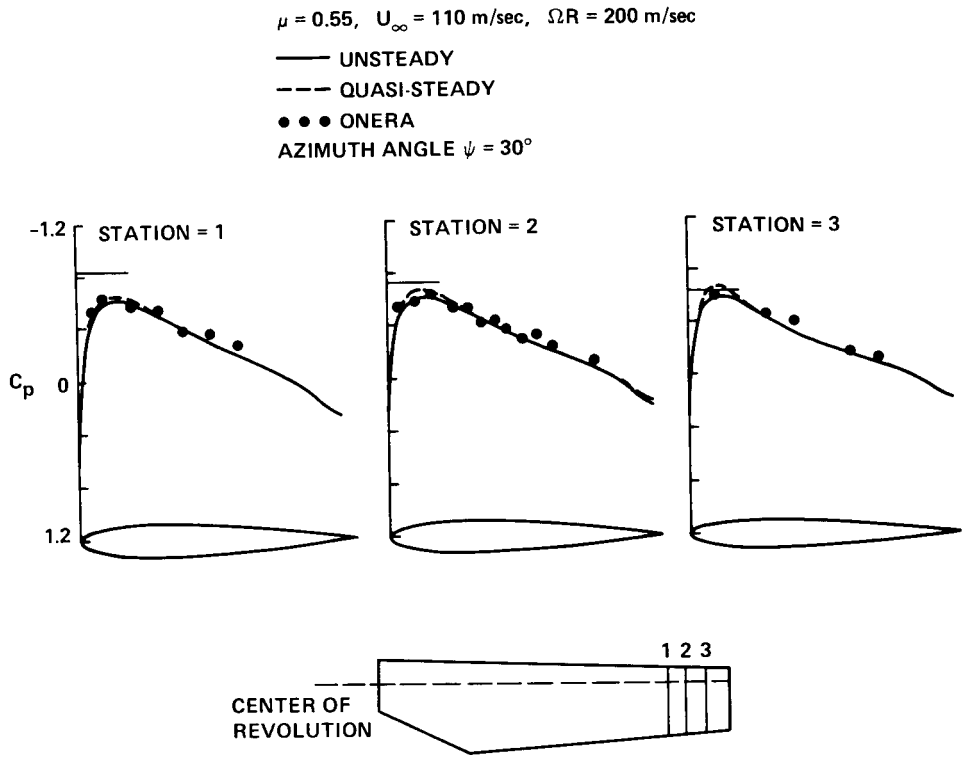

(a) Azimuth angle 30°.

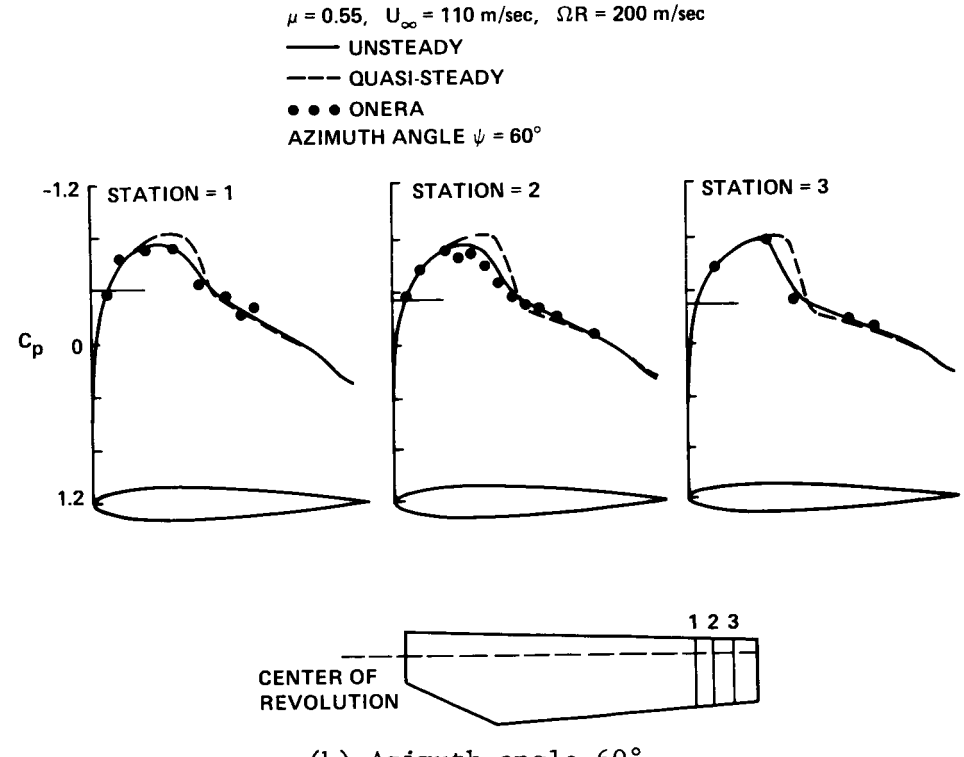

(b) Azimuth angle 60°.

Figure 3.- Unsteady effect. Comparison among unsteady and quasi-steady calculated, and measured, surface-pressure distributions at three span stations near the tip of a model rotor blade.

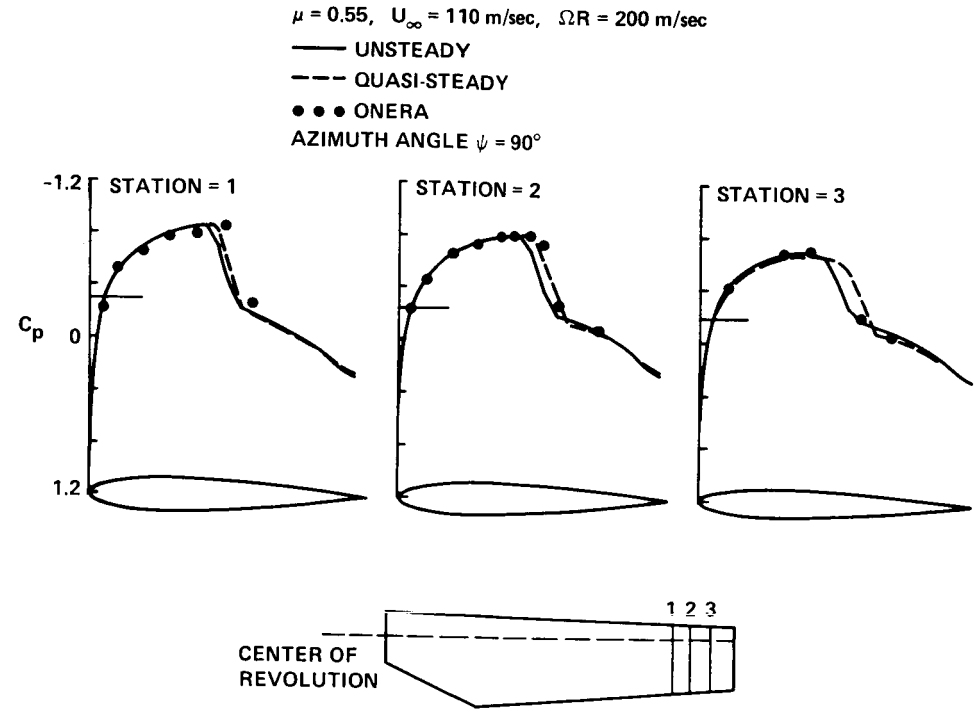

(c) Azimuth angle 90°.

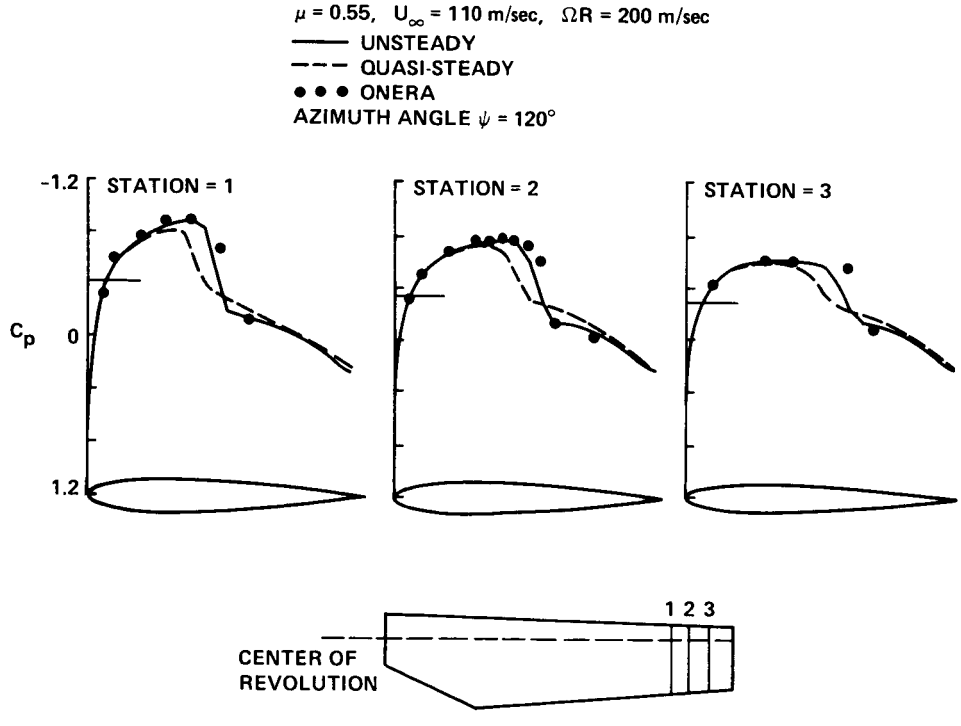

(d) Azimuth angle 120°.

Figure 3.- Continued.

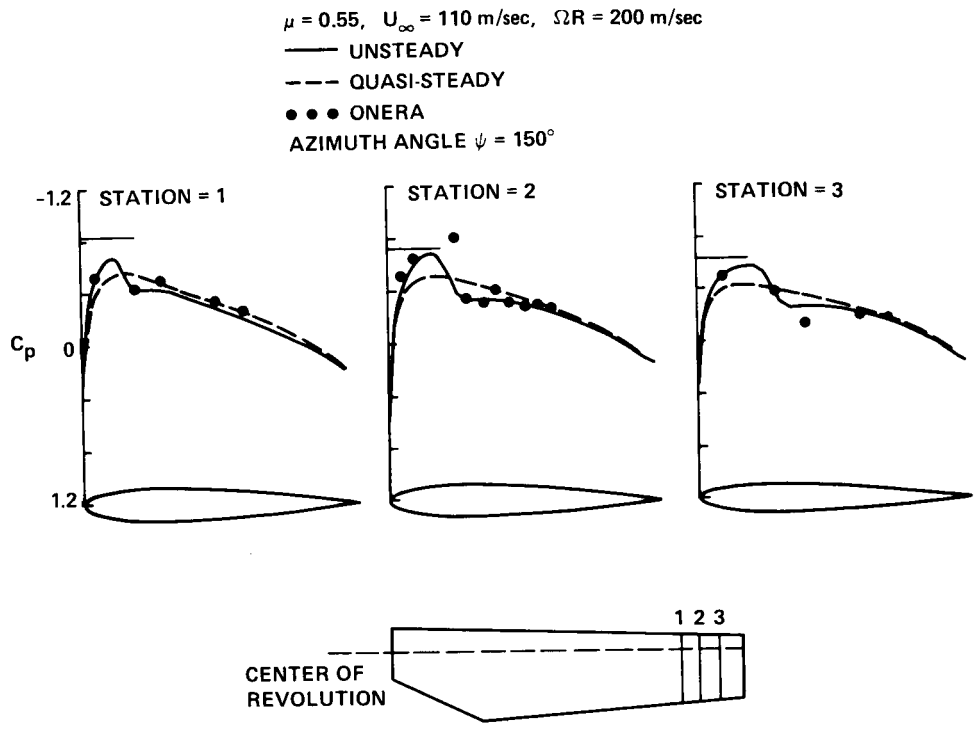

(e) Azimuth angle 150°.

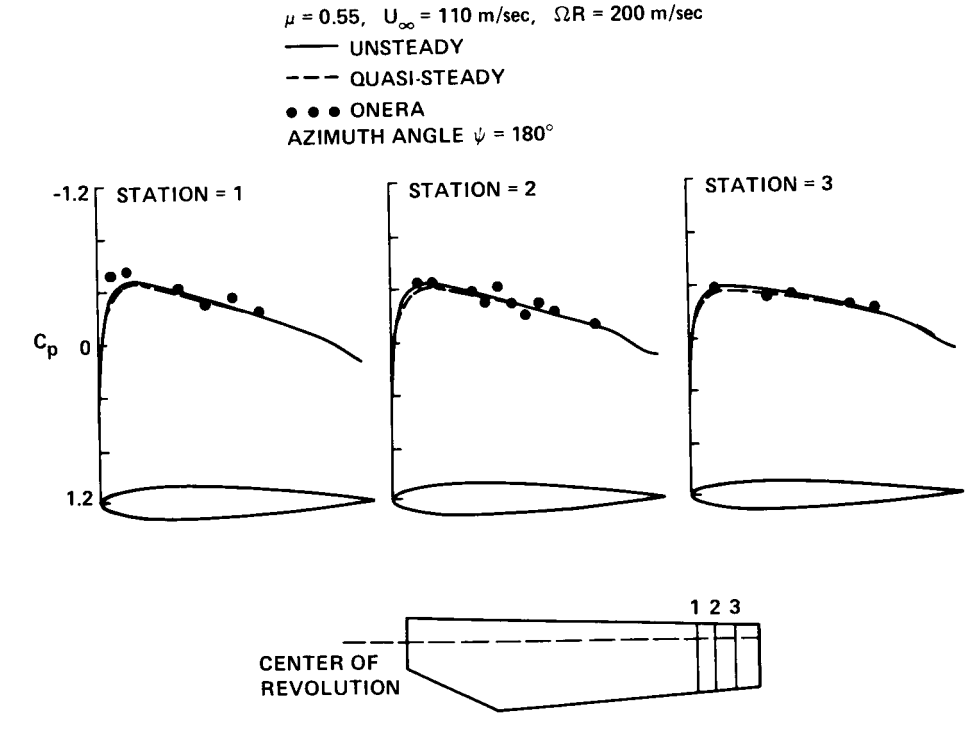

(f) Azimuth angle 180°.

Figure 3.- Concluded.

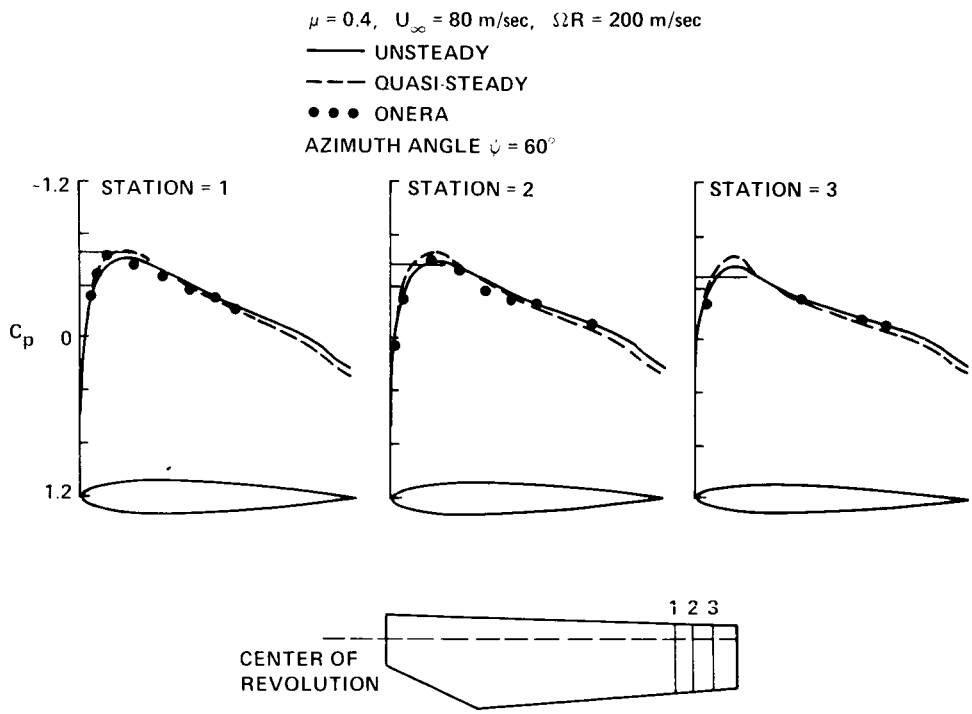

(a) Azimuth angle 60°.

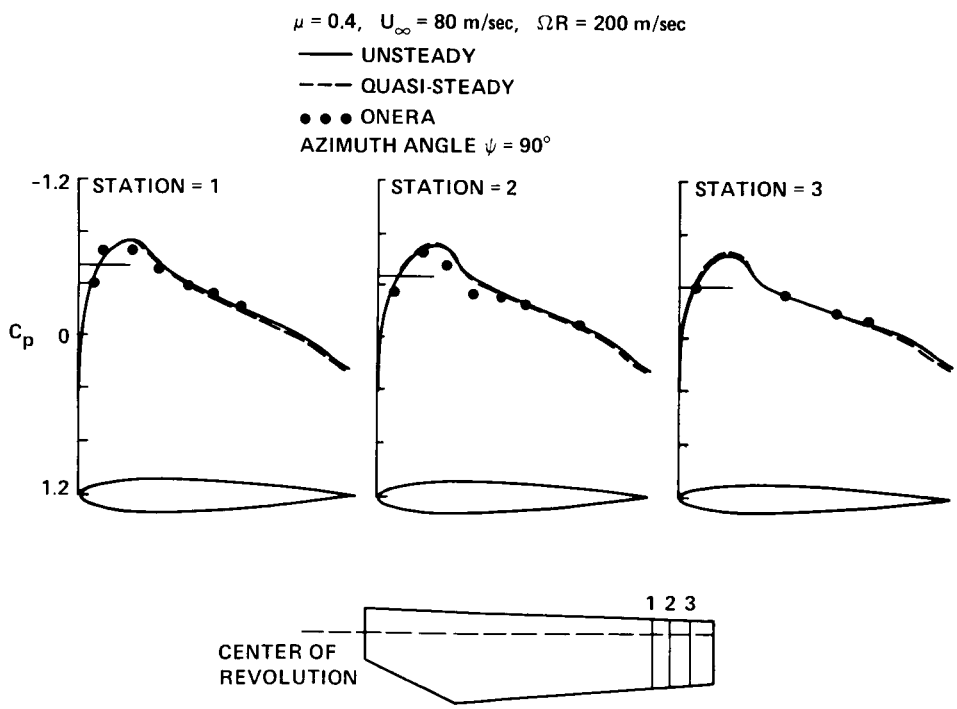

(b) Azimuth angle 90°.

Figure 4.- Assessment of the quasi-steady theory. Comparison among quasi-steady and unsteady calculated, and measured, surface-pressure distributions at three span stations near the tip of a model rotor blade.

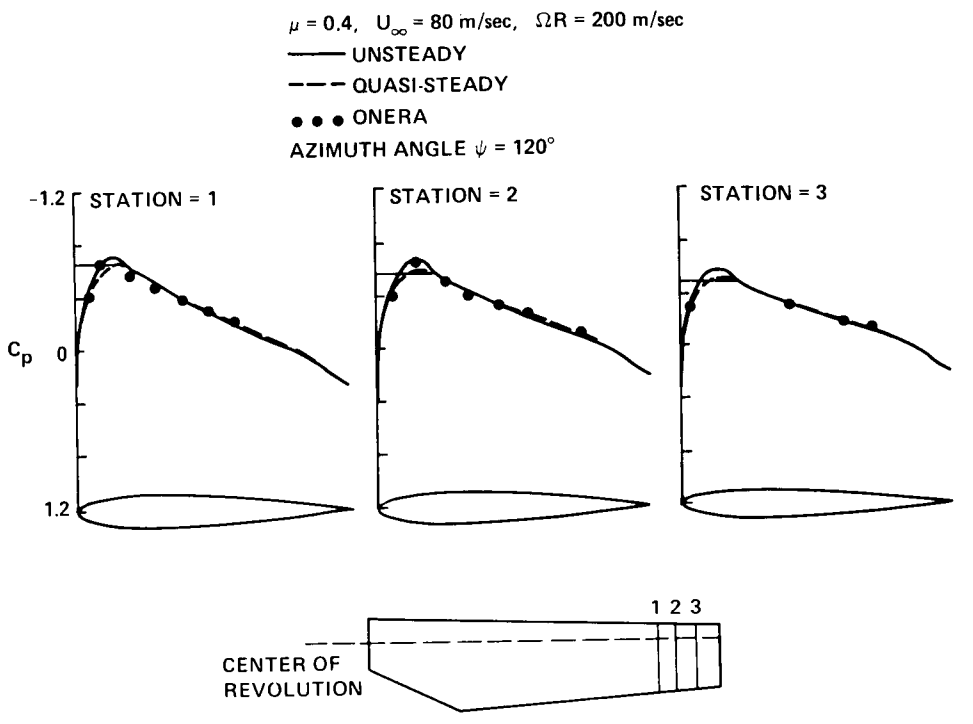

(c) Azimuth angle 120°.

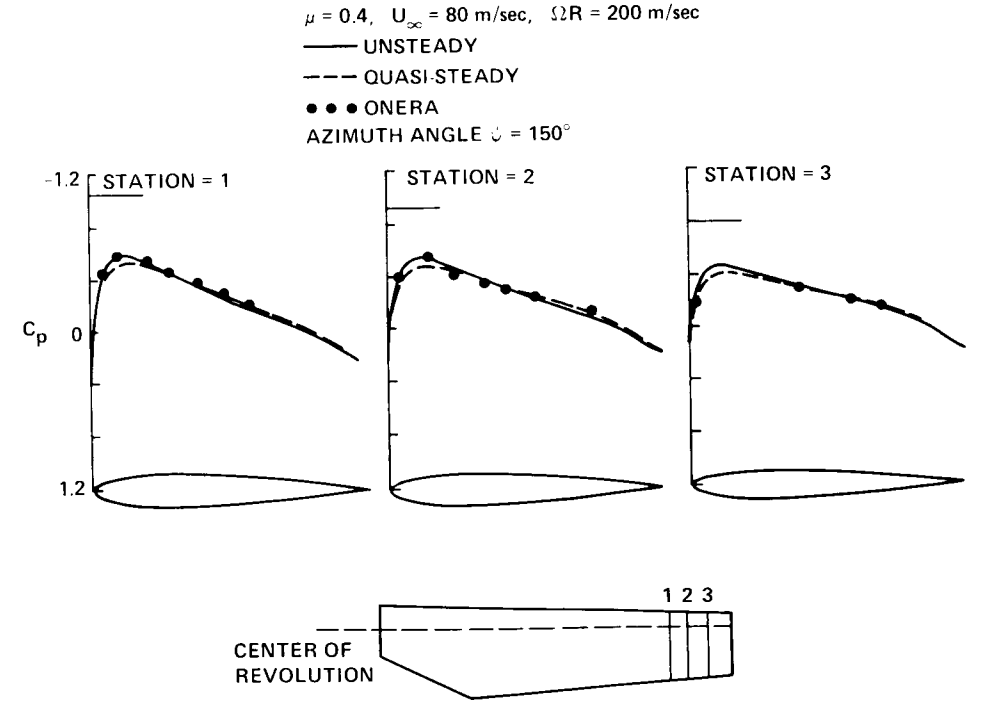

(d) Azimuth angle 150°.

Figure 4.- Concluded.

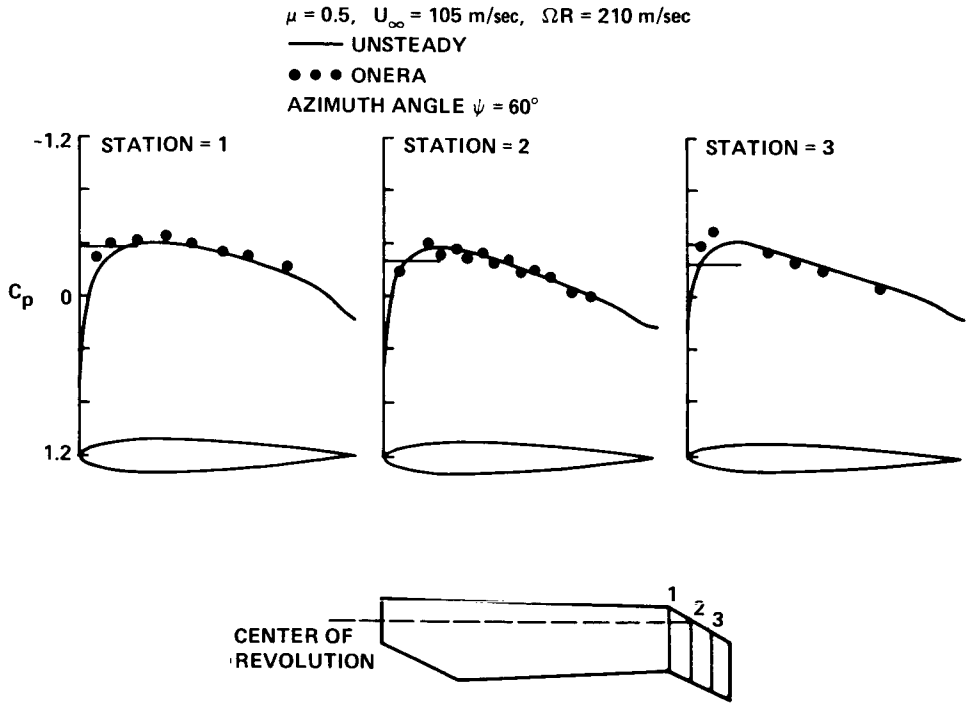

(a) Azimuth angle 60°.

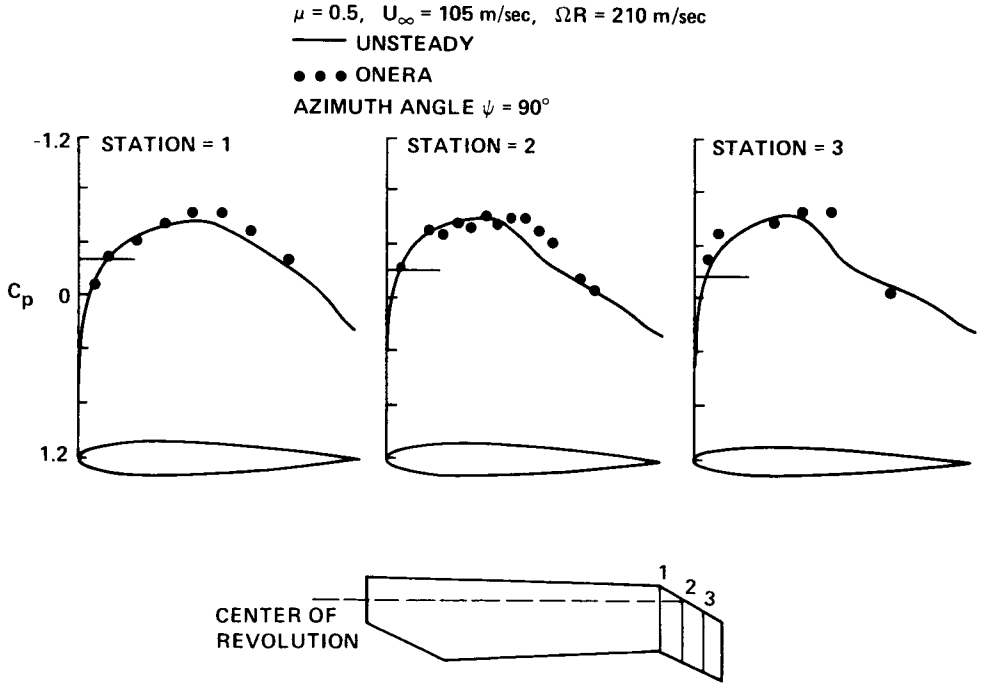

(b) Azimuth angle 90°.

Figure 5.- Planform effect. Comparison between unsteady calculated and measured, surface-pressure distributions at three span stations near the tip of a swept-tip (back 30°) model rotor blade.

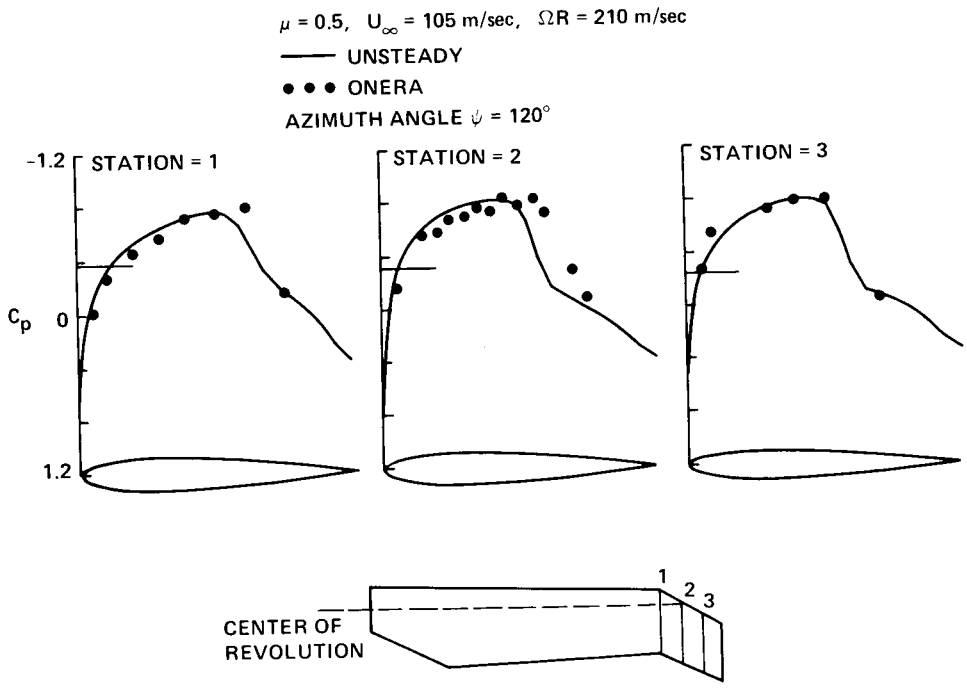

(c) Azimuth angle 120°.

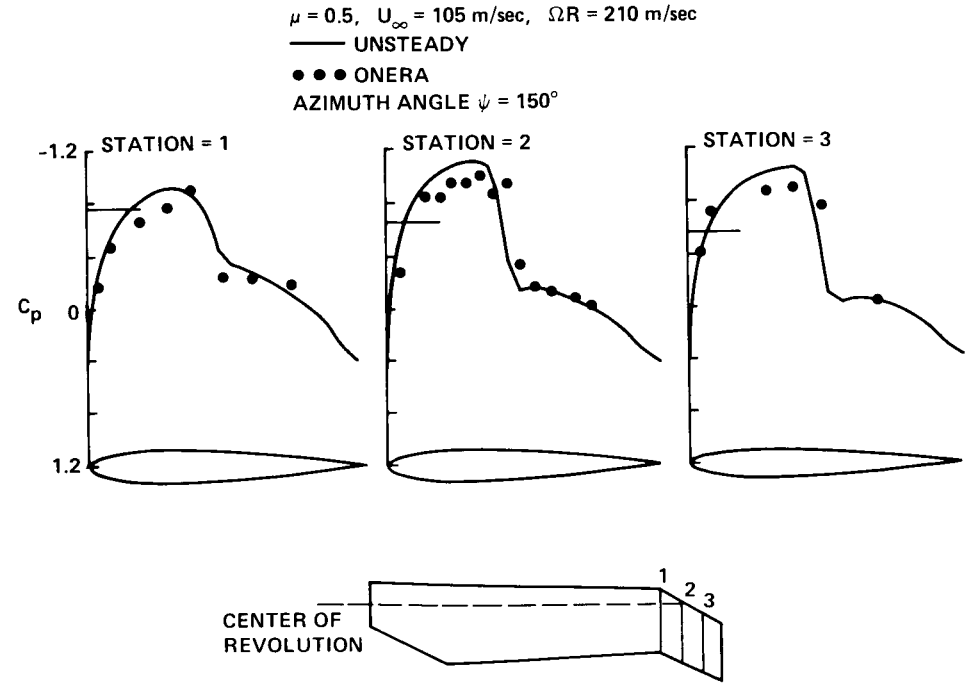

(d) Azimuth angle 150°.

Figure 5.- Continued.

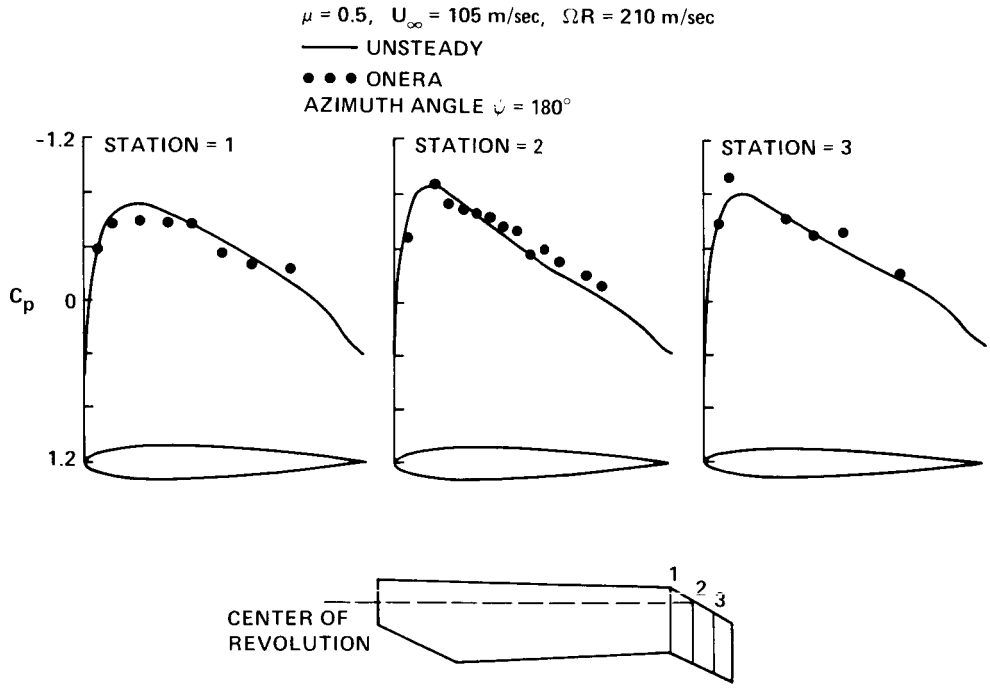

(e) Azimuth angle 180°.

Figure 5.- Concluded.

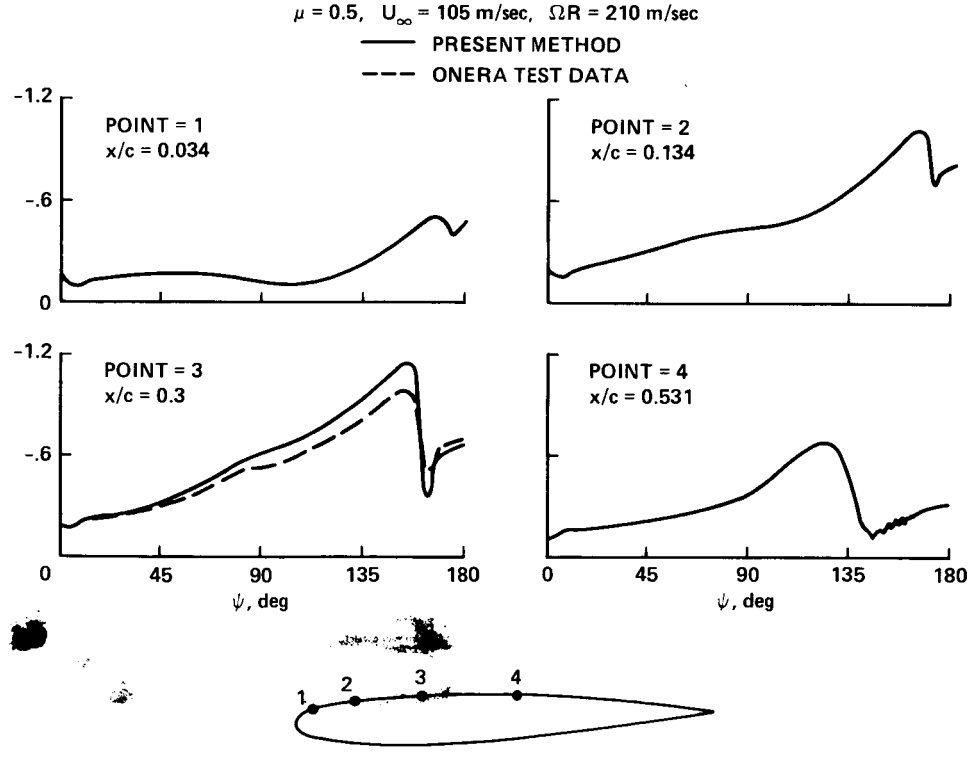

Figure 6.- Azimuthal pressure evolution on a swept-tip rotor blade.

1. Report No.	2. Government Accession No.	3. Recipient's Catalog No.
NASA TP-2375		

4. Title and Subtitle	5. Report Date
TRANSONIC FLOW ANALYSIS FOR ROTORS. PART 2 - THREE-DIMENSIONAL, UNSTEADY, FULL-POTENTIAL CALCULATION	January 1985
	6. Performing Organization Code
7. Author(s)	8. Performing Organization Report No.
I-Chung Chang	A-9682
	10. Work Unit No.
9. Performing Organization Name and Address	T-3414Y
Ames Research Center Moffett Field, CA 94035	11. Contract or Grant No.
	13. Type of Report and Period Covered
12. Sponsoring Agency Name and Address	Technical Paper
National Aeronautics and Space Administration Washington, DC 20546	14. Sponsoring Agency Code 505-42-11

15. Supplementary Notes

Point of contact: I-Chung Chang, Ames Research Center, MS 227-8
Moffett Field, CA 94035, (415) 965-6396 or FTS 448-6396

16. Abstract

A numerical method is presented for calculating the three-dimensional unsteady, transonic flow past a helicopter rotor blade of arbitrary geometry. The method solves the full-potential equations in a blade-fixed frame of reference by a time-marching implicit scheme. At the far-field, a set of first-order radiation conditions is imposed, thus minimizing the reflection of outgoing wavelets from computational boundaries. Computed results are presented to highlight radial flow effects in three dimensions, to compare surface pressure distributions to quasi-steady predictions, and to predict the flow field on a swept-tip blade. The results agree well with experimental data for both straight- and swept-tip blade geometries.

17. Key Words (Suggested by Author(s))	18. Distribution Statement
Aerodynamics Transonic flow Helicopter aerodynamics Unsteady flow Numerical analysis	[redacted] Subject Category 02

19. Security Classif. (of this report)	20. Security Classif. (of this page)	21. No. of Pages	22 Price
Unclassified	Unclassified	27	

NASA-Langley, 1984